Negative refraction imaging of acoustic waves by a two-dimensional three-component phononic crystal

Jing Li, Zhengyou Liu,* and Chunyin Qiu
Department of Physics, Wuhan University, Wuhan 430072, China
(Received 6 September 2005; revised manuscript received 6 December 2005; published 1 February 2006)

By using the multiple scattering methods, we extend the study of negative refraction imaging effect to two-dimensional three-component phononic crystal consisting of square arrays of coated cylinders in liquid. We show that based on localized resonance mechanism, the first band of the phononic crystal is strongly depressed, which gives rise to circular constant frequency surfaces. The negative refraction and left-handed behaviors are demonstrated by simulation of a Gaussian beam through a finite system. High-quality far-field imaging by a superlens with a refractive index $n=-1$ is realized, which follows the well-known wave-beam negative refraction law. This three-component phononic crystal may thus serve as a good acoustic device in negative refractive imaging.

DOI: 10.1103/PhysRevB.73.054302 PACS number(s): 43.20.+g, 43.58.+z, 78.20.Ci

I. INTRODUCTION

During the past few years, the negative refraction of electromagnetic waves in a left-handed material has attracted much interest.[1–5] The positive refractive index of the conventional optical lenses means that they need curved surfaces to form an image, whereas a negative refraction index allows a flat slab of a material to focus electromagnetic waves to a real image and behave as a superlens, from which numerous applications in science and medicine can be expected. There are two kinds of cases for negative refraction occurring in photonic crystals, the first case has the similar left-handed behavior as in the metamaterials possessing the simultaneous negative permittivity ε and negative permeability μ.[6] In this case, $\vec{k}$, $\vec{E}$, and $\vec{H}$ form a left-handed set of vectors, i.e., $\vec{S}\cdot\vec{k}<0$, where $\vec{S}$ is the Poynting vector, and $\vec{k}$ is the wave vector. Another is due to the negative-definite photonic effective mass,[7,8] in this case, the photonic crystals have an effective refractive index controlled by the band structure, and are behaving much like a uniform right-handed medium, i.e., $\vec{S}\cdot\vec{k}>0$. The negative refraction can be realized without employing a negative index or a backward wave effect.

Analogous phenomena for acoustic waves in phononic crystals are also of great significance. Recently, it is exhibited that the negative refraction behavior and imaging effect for acoustic waves can be observed in the phononic crystal consisting of square arrays of rigid or liquid cylinders placed in an air background.[9] The advantage to realizing the negative refraction imaging in the first band is that only the single mode in the first band can be excited in the crystals by the incident waves, meanwhile higher transmission can be guaranteed. However, due to the anisotropy of dispersion for the first band, images can only form in a near-field region. Very recently, Qiu *et al.* realized far-field imaging in a two-dimensional phononic crystal consisting of hexagonal arrays of steel cylinders in air, which takes advantage of the negative refractive behavior at the second band. Although the refractive index of $n\approx-1$ is indeed obtained when the filling ratio is increased to an extremely high value, the low transmission resulting from the high filling ratio keeps out more extensive applications.[10] Recently, Hu *et al.* showed that a high-quality far-field imaging can be realized in square arrays of silver nanowires in air for transverse-electromagnetic waves.[11] By using a metal-in-dielectric configuration, the first band is depressed, and a circular M-centered equivalent frequency surface (EFS) was thus obtained at the first band. Far-field focusing and imaging have also been realized by a square photonic crystal through choosing suitable scatterers for the lowest valence band.[12] We noted that there has been no parallel progress reported for the similar problem for phononic crystals. Could we find a circular M-centered EFS at the first band in phononic crystals with a square lattice?

The previous study of imaging in phononic crystals is mainly limited to two-component systems, and the conditions of imaging concern the appropriate intrinsic parameters of the two chosen components, such as the mass density contrast, the velocity contrast, the volume filling fraction, and the lattice structure. The recent work of Liu *et al.* demonstrates that there exist band gaps at extremely low frequencies based on the three-dimensional localized resonance structure units, in which a soft coating layer is introduced.[13–15] Similar results were also reported for a two-dimensional three-component system by Goffaux[16,17] *et al.* and by Platts *et al.*[18] It means that, based on the localized resonance mechanism, the low-lying flat first band can be expected in a two-dimensional three-component phononic crystal without an extremely high filling ratio, which is available to achieve a circular M-centered EFS, meanwhile guarantees a high transmittance for a superlens made from the crystal.

In this paper, we extend the study of a negative refraction imaging effect to two-dimensional three-component phononic crystals consisting of square arrays of coated cylinders placed in liquid. We show that the first band can be strongly depressed based on localized resonance mechanism, from which a circular M-centered EFS is indeed obtained. The negative refraction and left-handed behaviors are demonstrated by simulation of a Gaussian beam through a slab of the phononic crystal. Good-quality far-field imaging with a refractive index $n=-1$, which explicitly follows the well-

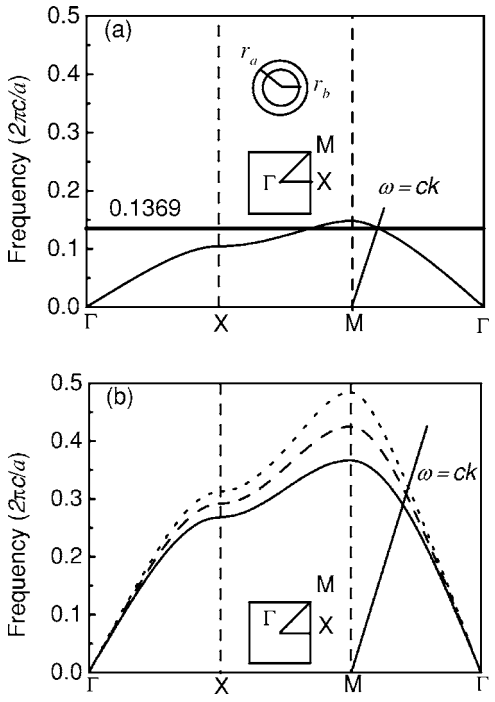

FIG. 1. (a) The first band for the phononic crystal consisting of the rubber-coated tungsten cylinders arranged in the square lattice in water. The filling fraction of the coated cylinders is 0.58, with $r_b/r_a=0.928$. The straight line beginning at point M represents the dispersion relation for water, and the horizontal line marks frequency 0.1369. (b) The first band for the phononic crystal consisting of tungsten cylinders arranged in the square lattice in water, the dotted, dashed, and solid curves are for filling ratios of 0.58, 0.68, and 0.75, respectively. The insets show the Brillouin zone of a square lattice. The frequency is in units of $2\pi c/a$, with c being the wave velocity in water and a being the lattice constant.

known wave-beam negative refraction law, can be realized at a frequency in the first band. Throughout the paper, a rigorous multiple scattering method (MST) (Refs. 19 and 20) is used to calculate the band structures and to perform numerical simulations for wave propagating in the finite real space.

II. NUMERICAL RESULTS AND DISCUSSIONS

The phononic crystal we consider here consists of the rubber-coated tungsten cylinders placed in water as a square lattice. The elastic parameters of the materials are as follows $\rho=19.3$ g/cm^3, $c_l=5.09$ km/s, $c_t=2.8$ km/s for tungsten; $\rho=1.3$ g/cm^3, $c_l=0.2$ km/s, $c_t=0.04$ km/s for rubber; $\rho=1.0$ g/cm^3, $c=1.49$ km/s for water, where ρ, c_l, and c_t are, respectively, the density, the longitudinal, and transverse sound velocity. The filling fraction of the coated cylinders (core plus coating layer) is fixed at 0.58. The inner and outer radius ratio of the coating layer, r_b/r_a, is fixed at 0.928, which follows that $r_a=0.429a$ and $r_b=0.398a$. Figure 1(a) shows the band structure of the three-component system (only the first band is given), which is obtained by using the MST method. In the calculation, the cutoff for the cylindrical wave expansion in the MST calculation is taken to be 4, and the convergence is tested with bigger cutoffs; we find that excellent convergence has been achieved for the cutoff being 4. From Fig. 1(a), it is observed that the first band is low lying with a rather flat top. Such features of the band are important in applications of phononic crystal as lens. First, a low-lying band can generally guarantee high wave transmission as required in applications; Second, a nearly flat band top is, geometrically, easier to achieve a circular EFS, which can guarantee the so-called all-angle negative refraction (AANR). AANR means that negative refraction takes place for incidence at an arbitrary angle. A circular EFS also makes the negative effective refractive index definable, which means that for an incidence at any angle, there is a constant effective refractive index. What is more, a nearly flat band top is geometrically easier to realize a circular EFS with the same big radius as that for the matrix medium (here, water), which gives rise to an effective refractive index of $n=-1$, and is important for far-field imaging.[10] In Fig. 1(a), we also depict the dispersion curve for water, a straight line beginning from M in the figure, which cuts the first band at a very low frequency 0.1369 (in unit of $2\pi c/a$, where a is the lattice constant, c is the sound velocity in water, the frequency corresponding to a wavelength of $\lambda=7.3a$), we observe that the dispersion curve around (and above) this frequency in the first band shows good symmetry reference to the vertical dashed line beginning at M point; this feature is important to obtain a circular EFS with the radius the same big as that for the water at around the M point, and achieve a negative effective refractive index of $n=-1$, as will be seen in the following. Before going further with this three-component system, we now turn to have a look over the two-component counterparts in order to have a comparison. Figure 1(b) shows dispersion curves for the corresponding two-component system consisting of pure tungsten cylinders in water for three increasing filling fraction, i.e., 0.58, 0.68, 0.75, respectively. We see that the first band cannot be depressed sufficiently by way of increasing the filling ratio, even to close packing. As a result, the symmetry as required for the dispersion curve to achieve a circular EFS at the frequencies around the intersection position of the dispersion curves for the phononic crystal and for water cannot be attained. From the comparison, we infer that the available first band achieved in the system with coating is ascribed to the coating layer. The tungsten core, rubber-coating layer together with the water background constitute the resonance unit, in which tungsten core provides the heavy mass and the soft rubber provides the soft spring. The conjunct influences of the resonance modes and the linear dispersion for an effective homogeneous medium result in the useful first band.

Now, let us examine the EFSs at frequency $0.1369(2\pi c/a)$ and some other frequencies nearby in the first band for the system with coating, which are shown in Fig. 2(a). It can be seen that at a frequency $0.1369(2\pi c/a)$, the EFS is approximately circular as anticipated, indicating that the phononic crystal can be regarded as a medium of an effective index of refraction, furthermore, the EFS is the same big as that for the water. Figure 2(a) also illustrates schematically the wave propagation directions in reciprocal space when the wave incident is from water to phononic crystal, while Fig. 2(b) illustrates a schematic diagram for the energy flux in real space. When a plane wave is incident

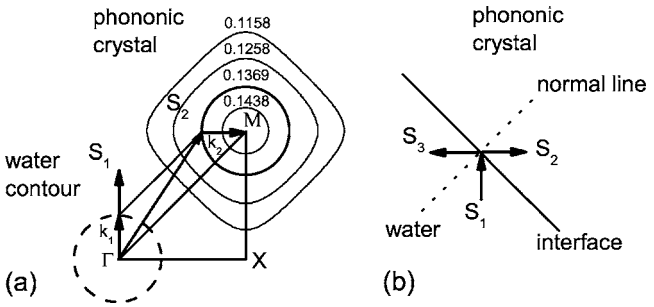

FIG. 2. (a) EFSs for some frequencies at the first band for the system with coating, moving inwards with increasing frequencies. The numbers in the figure mark the frequencies in units of $2\pi c/a$. Thick dashed and solid circles stand for the EFSs for water and for the phononic crystal at frequency $0.1369(2\pi c/a)$, respectively. For an incident plane wave with wave vector k_1 and energy flux S_1 in the water, the Bloch wave with wave vector k_2 and energy flux S_2 is excited in the phononic crystal. (b) Schematic energy flow diagram illustrates the propagation of the wave from water to phononic crystal in real space; S_3 is the reflected energy flux.

from water to a phononic crystal, the refracted modes are determined by the conservation of the wave vector component parallel to the interface, and the direction of the refracted wave inside the phononic crystal can be determined from the normal of the circular EFS.[6,7,21] So at frequency $0.1369(2\pi c/a)$, the incident and refracted directions of the energy flows will be mirror symmetric on the interface, i.e., the refracted energy flux has always a refraction angle the same as that of the incident energy, but located at the same side of the interface normal, as if the phononic crystal has a negative effective refractive index of $n=-1$.

We have shown that the circular EFS can be easily achieved by the band top flatness feature of the first band; the transmission coefficient for the phononic crystal with finite thickness at frequency 0.1369 is also readily high because of the low-lying feature of the first band. A simple calculation based on the layered MST (Ref. 22) with the cutoff for the cylindrical wave expansion being 4 show that the amplitude transmission coefficient can reach 0.770 for a 9-layer sample when the wave is incident on the sample along the surface normal, i.e., the [11] direction of the phononic crystal, much bigger than 0.022 for a 9-layer sample with the cylinders in the crystal almost close packed in the corresponding work by Qiu *et al.*[10] It shows that by using the three-component system, the transmittance through the crystal slab is greatly improved.

To demonstrate the negative refraction behavior of acoustic waves occurring at the interface of the phononic crystal and background medium, we simulate the displacement field generated by a Gaussian beam incident onto a phononic crystal slab. The sample is a 13-layer slab with the surface normal along the ΓM direction. The Gaussian beam with frequency $0.1369(2\pi c/a)$ is incident with an angle $\alpha=45°$, since the phononic crystal has an effective refractive index $n=-1$ at frequency $0.1369(2\pi c/a)$, the refracted beam should be expected to observe at the refraction angle $\beta=-45°$ according to the Snell's law. We give the simulation result in Fig. 3, from which we find that there exhibit obvi-

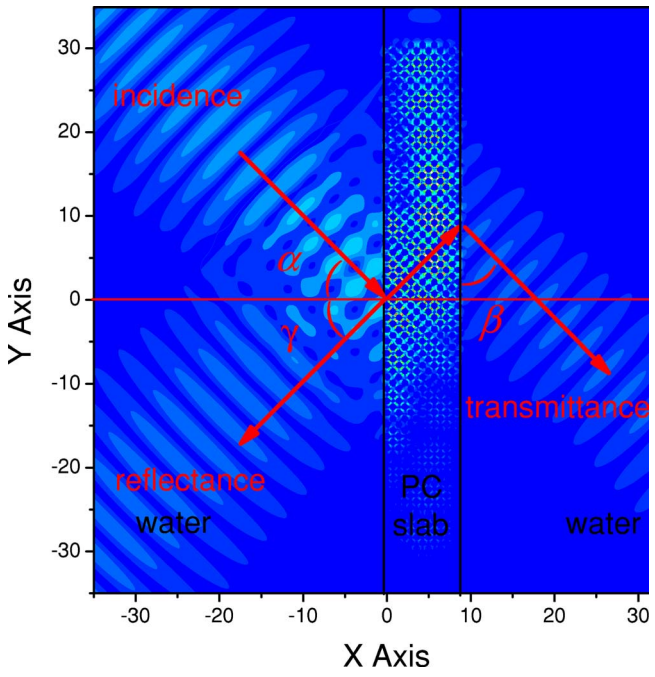

FIG. 3. (Color online) Displacement field patterns generated by an incident Gaussian beam on a 13-layer phononic crystal slab. The propagation directions of the Gaussian beam are marked by arrows, with α, β, and γ denoting the incident, refractive, and reflective angles. The scale is in units of a, the lattice constant. The vertical gray lines mark the slab surfaces.

ous negative refraction behaviors at the two interfaces of the slab. The refractive angle can be indeed approximately evaluated as $\beta\approx-45°$ in accord with the above prediction. Furthermore, reflectance by the left surface occurs due to a mismatch between the phononic crystal and water. The reflective angle can be approximately evaluated as $\gamma\approx45°$, which is equal to the incident angle, consistent with the conventional reflection law.

Imaging is regarded as one of the important applications of negative refraction materials, below the imaging effects of acoustic waves by phononic crystals of negative refractive indices are investigated by numerical simulations. First of all, it is essential to know how acoustic waves propagate through a slab of material with negative effective refractive index $n=-1$. Figure 4 schematically shows how the acoustic waves emitted from a point source propagate through a phononic crystal slab of a negative refraction index $n=-1$, and a thickness L, placed in a positive refraction index background (with $n=1$). A point source is placed on the left side of the slab, with a distance U from the left side surface. An image is obtained on the right side of the slab, with a distance V from the right side surface. Imaging with $U+V=L$ can be expected by a slab of such phononic crystal as a result of its characteristic of $n=-1$. Our simulation particularly gives the intensity distributions of the displacement field of the imaging effect. Two slabs with 11 and 15 layers of coating cylinders are shown in Fig. 5. We can see that the acoustic waves radiated from the point source on the left side of the slab, transmit through the slab, and focus onto a far-field

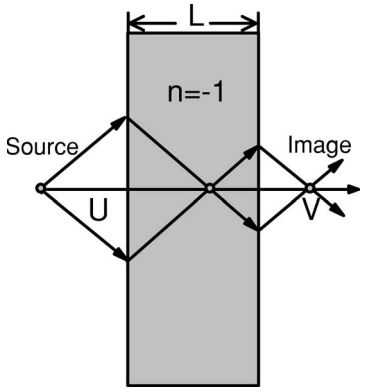

FIG. 4. Schematic imaging of a source by a slab of the material with negative effective refractive index $n=-1$.

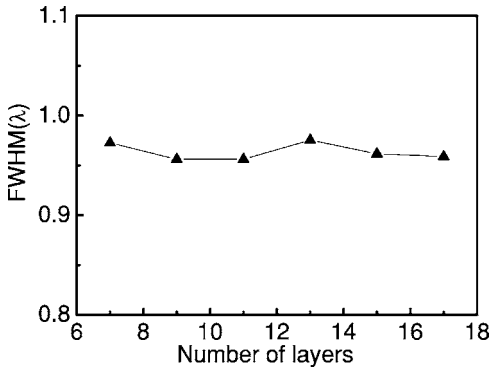

FIG. 6. The full widths at half maximum (FWHM) of the images vs the layer number of the slabs.

image on the right side finally. To check the formula $U+V=L$, we vary the distance of source to the left side of the slab U and check the distance of source to image H. For $n=-1$, we have known that $H=2L$. The thickness of 11-layer slab is $L=8.23a$, H are found to be $15.4a$ for $U_1=1.5a$, and $15.6a$ for $U_1=6.5a$, as shown in Figs. 5(a) and 5(b), respectively. For the 15-layer slab with thickness $L=11.05a$, H are found to be $22.2a$ for $U_2=1.5a$, and $22.0a$ for $U_2=9.5a$ as shown in Figs. 5(c) and 5(d), respectively. We have also checked the cases with various layer numbers and object lengths. It can be concluded that the imaging obeys fairly well wave-beam negative refraction law.

To get a further insight into the quality of imaging by the present system, we investigate the intensity distributions of displacement field at the image plane of the slabs with different layer numbers along the Y axis. In Fig. 6 we display the full widths at half maximum (FWHM) of the images vs the layer number of the slabs, which reveals a resolution comparable to the wavelength. As there is not a parallel mechanism (e.g., surface waves) as involved in the electromagnetic left-handed material lens,[23] the evanescent components cannot be recovered by the phononic crystal lens, this is the reason we do not observe a subwavelength resolution here. Furthermore, it is noted from Fig. 5 that the intensity distributions of displacement field on both the source and the image sides are almost in the same order of magnitude. The intensity distributions on the image side can be well read without amplification, which is superior to the corresponding work in the recent literature.[10] These results show that by using the three-component system, the transmittance through the crystal slab is improved while a good focus is available.

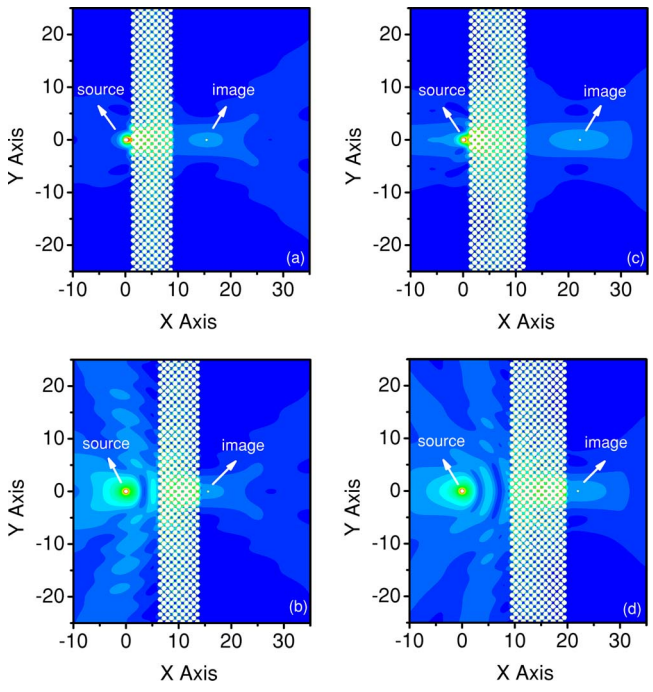

FIG. 5. (Color online) The intensity distributions of the displacement field of a point source and its image across an 11-layer slab with (a) $U_1=1.5a$ and (b) $U_1=6.5a$, and a 15-layer slab with (c) $U_2=1.5a$ and (d) $U_2=9.5a$, respectively, at frequency $0.1369(2\pi c/a)$.

In all the simulation discussed above, the cutoff for the cylindrical expansion in MST calculations is taken to be 4. To avoid the edge effect, all the sample models used in simulation have lengths (vertical dimension) bigger than $40\sqrt{2}a$. Bigger cutoff and lengths are used to test the accuracy of simulation, but no visible change in the field distribution can be observed, indicating excellent convergence.

III. CONCLUSION

In summary, through the exact simulation and physical analysis, we demonstrate the negative refraction and the imaging effects of two-dimensional three-component phononic crystal consisting of square arrays of coated cylinders in water. By comparison of the coated and uncoated systems, we found that the intrinsic localized resonance mechanism in the coated system accounts for providing the low-lying first band with the circular equivalent frequency surfaces, which is necessary for imaging by a slab of the crystal. The negative refraction is demonstrated by simulating a Gaussian beam through a slab of the phononic crystal, while the imaging of good quality, which follows the well-known wave-beam

negative refraction law, is demonstrated by simulating the acoustic waves radiated from a line source through a slab of the phononic crystal of $n=-1$. This three-component phononic crystal based on localized resonance mechanism may thus serve as a good acoustic device used in acoustic wave imaging.

ACKNOWLEDGMENTS

This work was supported by the National Natural Science Foundation of China (Grant Nos. 50425206, 10418014, and 10174054) and Doctoral Research Foundation of Ministry of Education of China (Grant No. 20020486013).

*Author to whom correspondence should be addressed. Email address: zyliu@whu.edu.cn

[1] V. G. Veselago, Sov. Phys. Usp. **10**, 509 (1968).
[2] J. B. Pendry, Phys. Rev. Lett. **85**, 3966 (2000).
[3] R. A. Shelby, D. R. Smith, and S. Schultz, Science **292**, 77 (2001).
[4] P. M. Valanju, R. M. Walser, and A. P. Valanju, Phys. Rev. Lett. **88**, 187401 (2002).
[5] A. A. Houck, J. B. Brock, and I. L. Chuang, Phys. Rev. Lett. **90**, 137401 (2003).
[6] M. Notomi, Phys. Rev. B **62**, 10696 (2000).
[7] C. Luo, S. G. Johnson, J. D. Joannopoulos, and J. B. Pendry, Phys. Rev. B **65**, 201104(R) (2002); Phys. Rev. B **68**, 045115 (2003).
[8] E. Cubukcu, K. Aydin, E. Ozbay, S. Foteinopoulou, and C. M. Soukoulis, Nature (London) **423**, 604 (2003).
[9] X. D. Zhang and Z. Liu, Appl. Phys. Lett. **85**, 341 (2004).
[10] C. Qiu, X. D. Zhang, and Z. Liu, Phys. Rev. B **71**, 054302 (2005).
[11] X. H. Hu and C. T. Chan, Appl. Phys. Lett. **85**, 1520 (2004).
[12] X. Zhang, Phys. Rev. E **71**, 037601 (2005).
[13] Z. Liu, X. X. Zhang, Y. Mao, Y. Y. Zhu, Z. Yang, C. T. Chan, and P. Sheng, Science **289**, 1734 (2000).
[14] Z. Liu, C. T. Chan, P. Sheng, A. L. Goertzen, and J. H. Page, Phys. Rev. B **62**, 2446 (2000).
[15] Z. Liu, C. T. Chan, and Ping Sheng, Phys. Rev. B **65**, 165116 (2002).
[16] C. Goffaux, J. Sanchez-Dehesa, A. L. Yeyati, Ph. Lambin, A. Khelif, J. O. Vasseur, and B. Djafari-Rouhani, Phys. Rev. Lett. **88**, 225502 (2002).
[17] C. Goffaux and J. Sanchez-Dehesa, Phys. Rev. B **67**, 144301 (2003).
[18] S. B. Platts and N. V. Movchan, *Proceedings of IUTAM Symposium on Asymptotics, Singularities and Homogenization in Problems of Mechanics* (Kluwer Academic, Dordrecht, 2003), pp. 63–71.
[19] J. Mei, Z. Liu, J. Shi, and D. Tian, Phys. Rev. B **67**, 245107 (2003).
[20] Y. Y. Chen and Z. Ye, Phys. Rev. E **64**, 036616 (2001).
[21] B. Gralak, S. Enoch, and G. Tayeb, J. Opt. Soc. Am. A **17**, 1012 (2000).
[22] C. Y. Qiu, Z. Y. Liu, J Mei, and J Shi, Solid State Commun. **134**, 765 (2005).
[23] V. A. Podolskiy and E. E Narimanov, Opt. Lett. **30**, 75 (2005).